GEOPHYSICS, VOL. 64, NO. 2 (MARCH-APRIL 1999); P. 403–416, 11 FIGS.

Estimating depth of investigation in dc resistivity and IP surveys

Douglas W. Oldenburg* and Yaoguo Li*

ABSTRACT

In this paper, the term "depth of investigation" refers generically to the depth below which surface data are insensitive to the value of the physical property of the earth. Estimates of this depth for dc resistivity and induced polarization (IP) surveys are essential when interpreting models obtained from any inversion because structure beneath that depth should not be interpreted geologically. We advocate carrying out a limited exploration of model space to generate a few models that have minimum structure and that differ substantially from the final model used for interpretation. Visual assessment of these models often provides answers about existence of deeper structures. Differences between the models can be quantified into a depth of investigation (DOI) index that can be displayed with the model used for interpretation. An explicit algorithm for evaluating the DOI is presented. The DOI curves are somewhat dependent upon the parameters used to generate the different models, but the results are robust enough to provide the user with a first-order estimate of a depth region below which the earth structure is no longer constrained by the data. This prevents overinterpretation of the inversion results. The DOI analysis reaffirms the generally accepted conclusions that different electrode array geometries have different depths of penetration. However, the differences between the inverted models for different electrode arrays are far less than differences in the pseudosection images. Field data from the Century deposit are inverted and presented with their DOI index.

INTRODUCTION

In a dc resistivity or induced polarization (IP) survey we are generally provided with data d (apparent resistivity or apparent chargeability) and an estimate of their errors. An inverse problem is then solved to find the model m (conductivity or chargeability) that generated the data. It is recognized that the inverse problem is nonunique, and modern strategies cope with this by using optimization techniques. Let ϕ_m be a functional of the model and let ϕ_d denote the misfit functional. The optimization problem is solved by finding a specific model m^* that minimizes ϕ_m subject to $\phi_d = \phi_d^*$, where ϕ_d^* is a target misfit. The nature of the constructed model is determined by ϕ_m, and much effort is required to tailor this functional so that m^* is interpretable, has the right "character," and is consistent with a priori knowledge about the earth. The amount of structure in m^* is determined by how well the observed data are reproduced. Generally, increasing the fit to the data requires more structure. When the minimization is complete, m^* is our best estimate of the true earth model, and it is from that image that we want to make geophysical and geological inferences. When viewing this image however, there are numerous questions that arise: (1) Which features in the recovered model emulate those in the true earth? (2) What confidence do we have in the existence of the features? (3) What is the level of detail that can be responsibly inferred? (4) Are there artifacts at depth, which if interpreted, would lead to misleading interpretations?

These questions are interrelated, but this paper focuses on artifacts at depth. Surface potentials measured in dc resistivity and IP surveys are sensitive to conductivity and chargeability only in a region in the vicinity of the electrode array. Yet when the data are inverted, it is necessary to consider a mathematical model that extends outwards from the survey area and to great depths. The boundaries are determined by the finite difference mesh used to carry out forward modeling, and they must be sufficiently far from the survey area so that imposed approximate boundary conditions do not cause numerical artifacts in the forward modeling. Because the recovered conductivity or chargeability extends to these boundaries, it is not known whether features observed at great depth are demanded by the data or if they are artifacts associated with the model objective function that is minimized.

To motivate our analysis, consider an attempt to recover a 2-D conductivity structure using a dc resistivity survey. In Figure 1, we show a synthetic model that has a variety of structure. On the left, one resistive and two conductive prisms are buried beneath highly conductive surface blocks in a

Manuscript received by the Editor October 31, 1997; revised manuscript received September 3, 1998.
*University of British Columbia, Department of Earth and Ocean Sciences, 129-2219 Main Mall, Vancouver, British Columbia V6T 1Z4, Canada. E-mail: doug@geop.ubc.ca, li@eos.ubc.ca.

homogenous earth. One prism extends to infinite depth. A vertical contact separates media of highly different conductivity; on the right, a circular-shaped Gaussian conductor is buried beneath a layer of random conductivity. A pole-dipole survey with $n = 1 \ldots 8$ and $a = 10$ m was simulated. The data, after being contaminated with 5% Gaussian noise, are shown in Figure 1b.

The data are inverted using the methodology outlined in Oldenburg and Li (1994). The model objective function ϕ_m is chosen to be a discretized version of

$$\phi_m(m) = \alpha_s \int_{area} (m - m_0)^2 dx\, dz + \alpha_x \int_{area} \left(\frac{d(m - m_0)}{dx} \right)^2 dx\, dz + \alpha_z \int_{area} \left(\frac{d(m - m_0)}{dz} \right)^2 dx\, dz, \qquad (1)$$

where $\alpha_s, \alpha_x, \alpha_z$ are constants, m_0 is a reference model, and $m = \log \sigma$. The misfit functional ϕ_d is

$$\phi_d = \sum_{i=1}^{N} \left(\frac{d_i^{obs} - d^{pred}}{\epsilon_i} \right)^2, \qquad (2)$$

where ϵ_i is the estimated standard deviation of the data. The model was divided into $M = 2500$ cells and the number of data $N = 316$. Minimizing equation (1) subject to $\phi_d = N$, its expected value, produces the model in Figure 1c. In carrying out the inversion, the reference model was specified to be a half-space of 400 ohm-m and $(\alpha_s, \alpha_x, \alpha_z) = (0.001, 1, 1)$.

The model in Figure 1c bears considerable likeness to the true model in Figure 1a. The surface inhomogeneities are well delineated, and the underlying conductive prisms are clearly visible. The vertical contact is sharply imaged but it extends only to limited depth. The variable surface layer is well defined, and the conductor rises distinctly above the resistive background. Overall, manifestations of all of the true structures are observed, but there are both minor and major differences between the images in Figures 1a and 1c. In the recovered model, amplitudes of anomalies are reduced and the boundaries of the recovered prisms are smooth. This is a consequence of using the ℓ_2–norm and minimizing $(dm/dx)^2$ and $(dm/dz)^2$. These discrepancies can be considered minor. Major differences between Figures 1a and 1c occur at the sides and at depth where the recovered resistivity returns to the a priori reference model. Conductive or resistive features in those areas do not significantly affect the data, and the inversion readily complies with its mandate to produce a simple model that is close to the background.

Of all of the discrepancies between Figures 1a and 1c, the truncation of the second conductor is perhaps the most

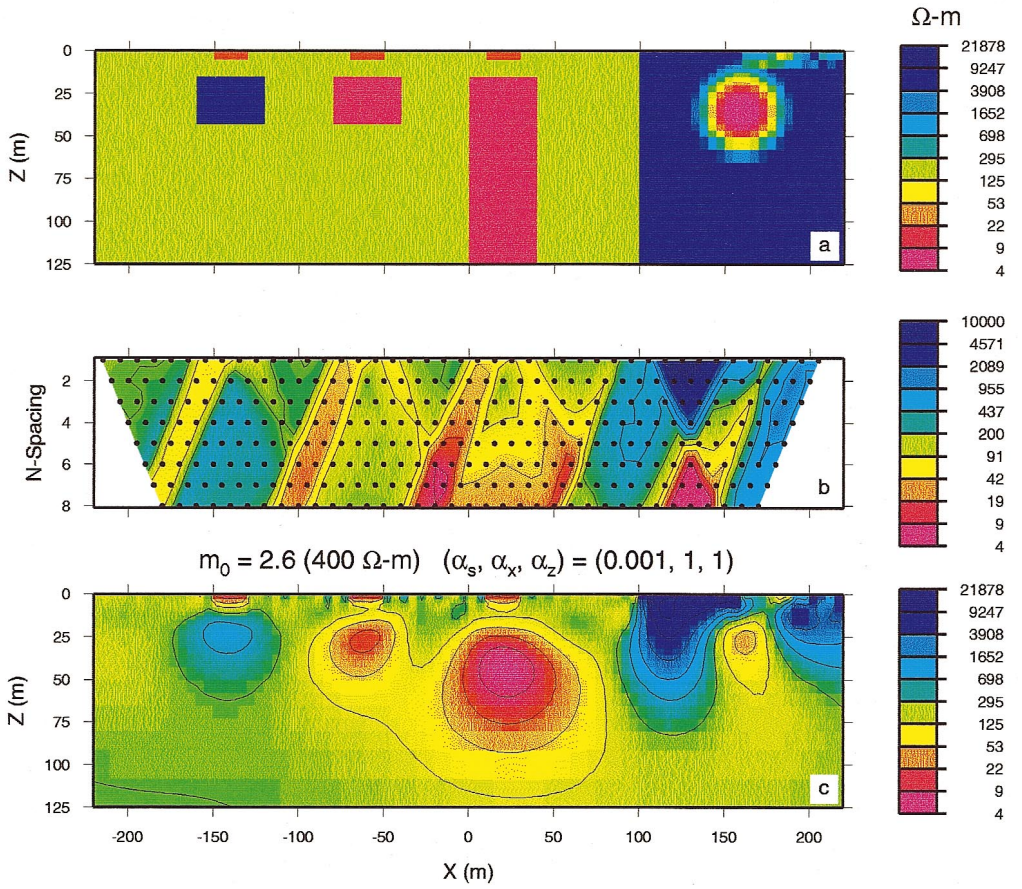

FIG. 1. (a) The synthetic resistivity model. (b) Error-contaminated data from a pole-dipole survey in which the potential dipole is on the right. The a spacing is 10 m, and $n = 1 \ldots 8$. (c) The recovered resistivity model.

important. If Figure 1c is believed, then the second conductor is wrongly inferred to have limited depth extent. In reality, the truncation is the result of a particular choice of ϕ_m and the fact that structure at depth no longer significantly affects the data. For interpretation of this inversion result, it is therefore necessary to delineate the depth below which the recovered model is no longer controlled by the data. That is the goal of this paper.

Before providing details of our approach, it is important obtain some insight about the nonuniqueness that is inherent in this inverse problem. We generate three additional models that fit the data to the same global misfit as in Figure (1c). The models in Figure 2 are respectively generated to be (a) close to a background, (b) horizontally continuous, and (c) vertically continuous. These are all poorer representations of the true earth model than that shown in Figure 1c. The predicted data from each model is shown in Figure 2. This example illustrates the importance of choosing the correct objective function when carrying out the optimization. It also suggests that quantifying the practical depth of investigation is not an easy problem that has a single unequivocal answer.

The paper is structured in the following manner. We first review current approaches for estimating depth of investigation (DOI). The next section shows how DOI information can be obtained by carrying out additional inversions. Two methods are presented. The choice of method depends upon the objective function that was used to generate the model that is to be interpreted. The depth of investigation for different arrays is then briefly examined for the test data set. We conclude with a field example and summary remarks.

APPROACHES TO QUANTIFYING DEPTH OF INVESTIGATION

For dc and IP surveys, the concept of "depth of investigation" has generally been associated with a depth to which the data are particularly sensitive. Barker (1989) provides a concise summary. Most approaches first compute a curve that indicates what proportion of the final measured signal arises from a thin layer at depth in a homogenous half-space. Either the depth at which the maximum occurs (e.g., Evjen, 1938; Roy and Apparao, 1971; Roy, 1972 or the depth of the median value (Edwards, 1977) can be used. The median is the depth at which half of the signal contribution comes from above and half from below. These analyses have given rise to various survey geometries championed by different groups. Investigation depths from Edwards (1977) are given as factors relative to the characteristic length of the array (dipole length in pole-dipole and dipole-dipole arrays, inter-electrode spacing in Wenner array, the distance between current and potential electrodes in pole-pole array). These depths, while helpful as guidelines in survey design, do not quantify the depth to which the features in the inverted model can be interpreted.

Other attempts to define a depth of investigation make use of forward modeling techniques and concentrate upon the question of whether the data are able to detect a body at depth (e.g., Van Nostrand, 1953; Apparao et al., 1992). A conductive or resistive feature is assumed at depth, and predicted data are compared to those obtained without the feature. If the assumed feature sufficiently alters the data, the depth of investigation is at least as deep as the top of the feature. This methodology is very useful in survey design, but it does not lend itself easily to quantifying depth of investigation as it relates to the model recovered from the field survey data.

Our depth of investigation seeks to determine the depth below which the data are no longer sensitive to the physical property. Simple rules of thumb are not expected to be applicable because the depth of investigation is highly dependent upon the conductivity structure, the acquisition geometry, and data errors. In an important paper, Parker (1984) showed that the potentials observed over a 1-D earth can be explained by a sequence of conductive layers whose accumulated thickness is infinitesimal. So without further information, the inferred depth of penetration is theoretically zero. Finite limits on depth of investigation can only be obtained by limiting the values of conductivity or the rate at which the conductivity changes with depth. It is not clear what aspects of Parker's analysis carry over to two dimensions, but the results in Figure 2 show that nonuniqueness in dc resistivity inversions is severe. It is likely, therefore, that inferences, obtained from a mathematical analysis that considers all models that reproduce the data, provide limited insight about the true depth of investigation. Usable information comes only when additional constraints, such as those required by the model objective function, are imposed upon the models.

To make practical progress, we restrict our analysis to models that are, in some sense, "close" to m^*, our preferred model. Although a Backus-Gilbert analysis (e.g., Oldenburg, 1978) can provide insight about resolving depths, it only considers models that are linearly close to m^*. This is too restrictive. In this paper, we generate models that have the same general characteristics as m^*, for example smoothness in horizontal and vertical directions, but yet differ substantially from m^*. The models are of interest in themselves and, with a minimum of computational effort, differences between the images can be used to illuminate the depth corridor where data no longer constrain earth structure.

DEPTH OF INVESTIGATION USING INVERSE MODELING

We assume that the user has defined a model objective function $\phi_m(\alpha_s, \alpha_x, \alpha_z, m_0)$ and has obtained a model m^* that minimizes ϕ_m subject to the data constraints. m^* represents the best estimate of the earth, and the next goal is to estimate the depth below which features seen on the image are no longer controlled by the data. We proceed by finding other models that fit the data to the same degree as m^*. This exploration of model space can be accomplished by altering the objective function and performing a subsequent inversion. Depending upon the parameters in ϕ_m there are two approaches.

Method 1: $\alpha_s > 0$, m_0 = constant

Assume that a half-space is chosen as a background reference model and that α_s is sufficiently large so that the first term in the objective function in equation (1) is of importance in the minimization. Evidence for this is that the constructed model returns to the half-space value at depth. This was observed in the inversion in Figure 1 where the reference model was 400 ohm-m. Figure 3 shows two other inversions in which

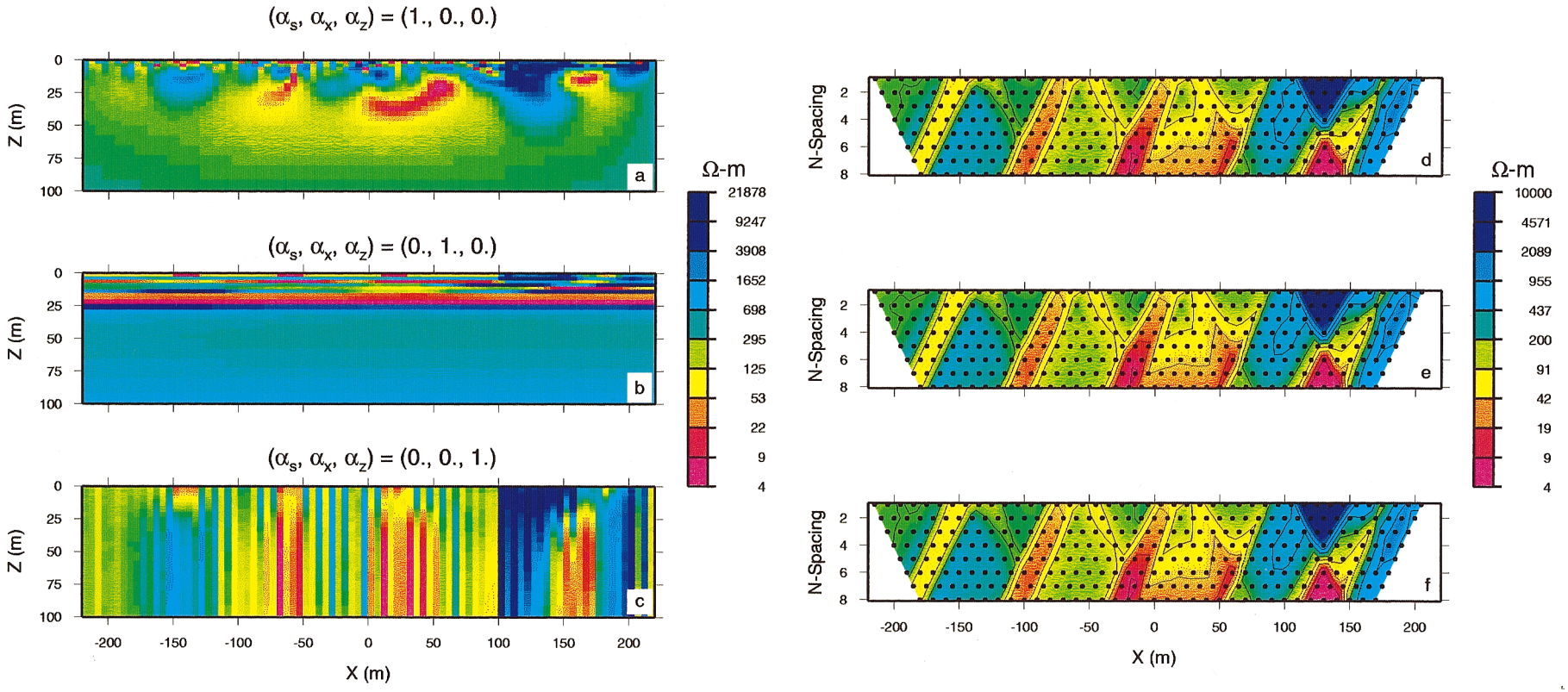

FIG. 2. Three resistivity models which reproduce the data in Figure 1: (a) the model which is close to a background resistivity of 400 ohm-m, (b) a model which has minimum structure in the horizontal direction, (c) a model which has minimum structure in the vertical direction. The predicted data for each inverted model is shown on the right. They can be compared with the observed data in Figure 1b.

the backgrounds are 4000 ohm-m and 40 ohm-m, respectively. There are clearly major differences in the images at depth. Quantifying those differences provides an estimate of DOI.

Consider two inversions carried out with constant reference models m_{1r}, m_{2r}. Let m_1, m_2 be the models recovered, and define

$$R(x,z) = \frac{m_1(x,z) - m_2(x,z)}{m_{1r} - m_{2r}}. \qquad (3)$$

R will approach zero at locations where the two inversions produce the same result regardless of the value of the reference model. We assign high credibility to those areas. R will approach unity at locations where the inversions achieve the value of the reference model. The data do not constrain the model and, hence, low credibility should be assigned to the model values in those areas. In Figure 4c, we plot R obtained from models in Figures 3a and 3c. We refer to this as the DOI index, and it is a companion plot to be used to aid interpretation of m^*. Features observed in Figure 1c that correspond to high DOI values should be omitted from the interpretation. This is facilitated by a contour plot of the DOI values superposed upon m^* as in Figure 3b. An alternative is to blank out that portion of the model for which R is greater than some value. The choice of what is a low or high value of DOI is arbitrary but not crucial. Once the DOI index begins its increase, it does so rather quickly. A reasonably cautious value might be 0.1 or 0.2.

A sharp boundary that characterizes DOI is extreme and not physical since our ability to see into the earth diminishes gradually with depth. This information can be presented by scaling the color intensity of the conductivity image m^* with the DOI value. Portions with large DOI values become invisible, and therefore they cannot distract from the visual interpretation. This is shown in Figure 4a.

Interpreting the conductivity model and the DOI information with a cutoff of $R = 0.1$ (or using Figure 4a) leads to the following conclusions. All buried bodies are likely of limited

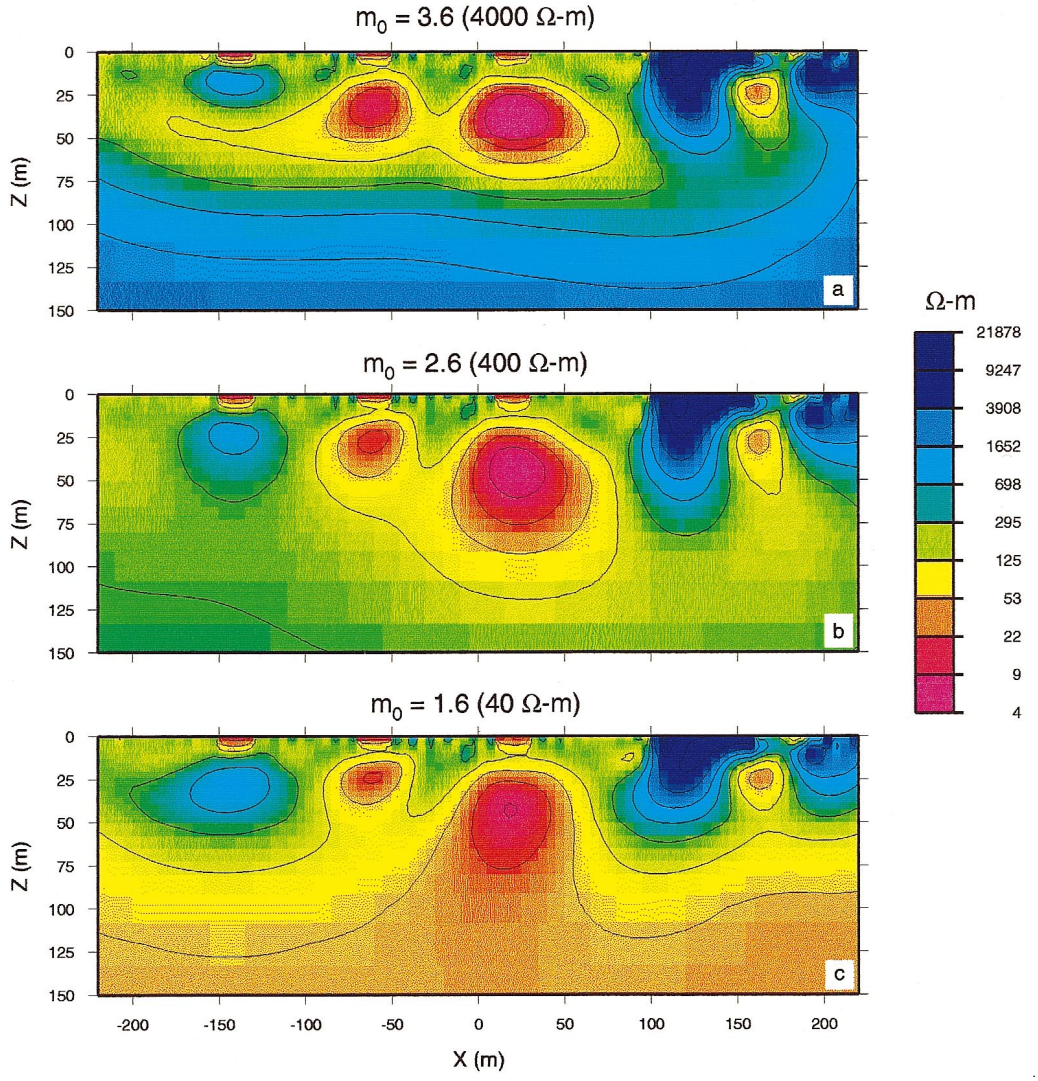

FIG. 3. Resistivity models generated with half-space reference models of (a) 4000 ohm-m, (b) 400 ohm-m, and (c) 40 ohm-m. All models fit the data in Figure 1b to the same chi-squared misfit. $(\alpha_s, \alpha_x, \alpha_z) = (0.001,\ 1,\ 1)$ for all inversions.

depth extent except for the larger conductor in the middle. That is the only body intersected by the $R = 0.1$ curve; the others exhibit considerable closure above the contour. In computing the DOI map in Figure 4, we took differences between models that were larger and smaller than 400 ohm-m. We refer to this as a two-sided difference. DOI maps obtained by taking only one-sided differences, that is, using reference halfspaces of 40 and 400 ohm-m and 400 and 4000 ohm-m were essentially the same as that shown in Figure 4.

Method 2: $\alpha_s = 0$

Inversions are sometimes completed by setting $\alpha_s = 0$ and minimizing structure in the horizontal and vertical directions. The resultant model will be independent of any reference halfspace and so equation (3) cannot be used. In practise, numerical considerations require that α_s not be set exactly to zero. Nevertheless it can be made small enough to provide the needed numerical stability without having significant effect on the recovered model. In Figure 5b, we present an inversion in which $\alpha_s = 10^{-6}$ and $m_0 = 2.6\,(400$ ohm-m). This model is now regarded as m^*, our best estimate of the earth model. We note that the resistivity at depth is a smoothly varying function.

To generate a conductivity model different from m^*, we keep $\alpha_s = 10^{-6}$ and introduce a reference $m_0 = \alpha + \gamma z$, where α is an average value of the near-surface log conductivity and γ is a constant. At sufficiently large depths, the depth derivative of the recovered model will asymptote to γ. Let m_1 and m_2 be two models constructed using reference models with slopes $+\gamma$ and $-\gamma$ respectively. These are shown in Figures 5a and 5c for a choice of $\gamma = 0.01$. The large conductor appears as a closed feature in Figure 5a and as a vertical protrusion connected to a large regional conductor in Figure 5c. The other bodies appear

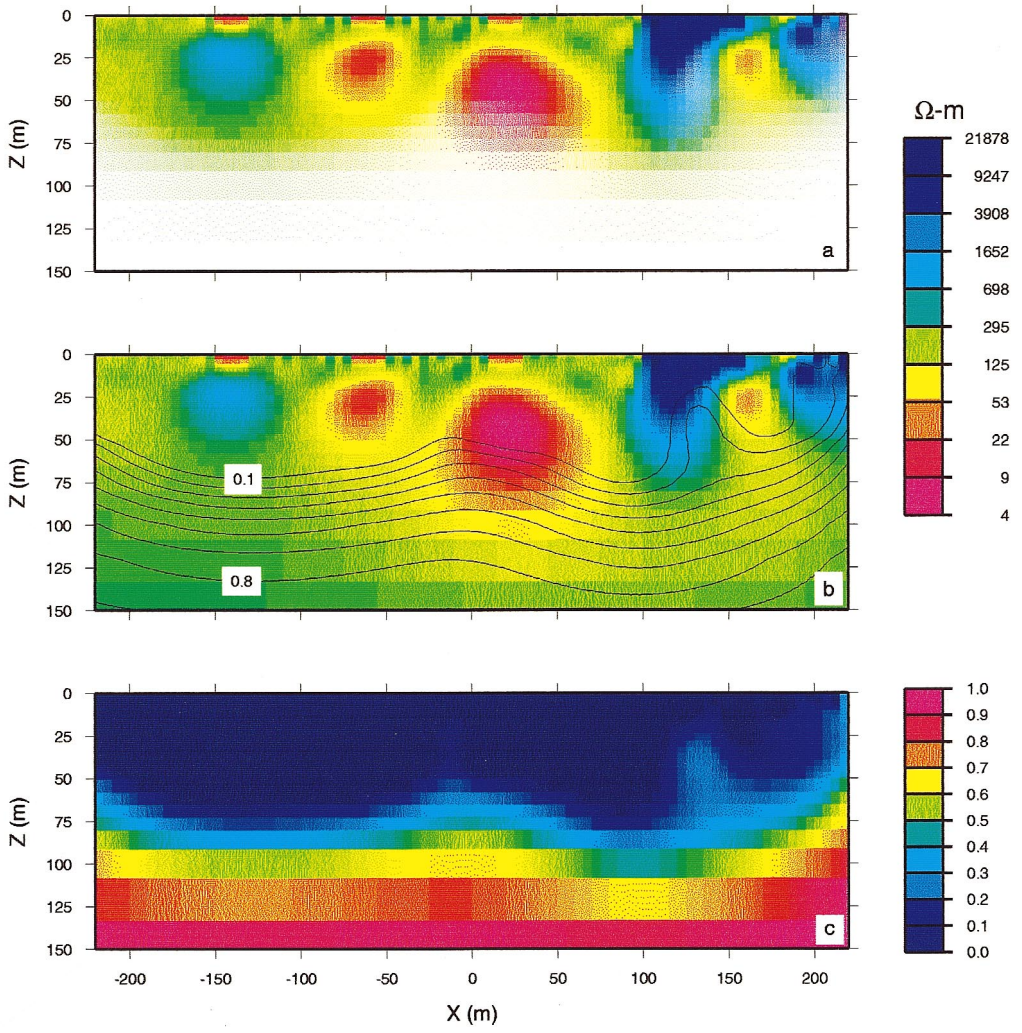

FIG. 4. The DOI index computed from inversions having reference backgrounds of 4000 ohm-m and 40 ohm-m is provided in (c). This information is superposed on m^* as contour lines in (b). The contour interval is 0.1. In (a) the intensity of m^* is scaled by the DOI value. White regions correspond to areas where the resistivity has minimal effect on the data.

to be confined. Differences between the two images can be evaluated using a cross-correlation. Let

$$C = \frac{\sum_i^n (m_{1i} - \bar{m}_1)(m_{2i} - \bar{m}_2)}{\left(\sum_i^n (m_{1i} - \bar{m}_1)^2 \sum_i^n (m_{2i} - \bar{m}_2)^2 \right)^{1/2}}, \quad (4)$$

where the sum is taken over n cells in a rectangular area centered around a cell, $\bar{m}_1$ is the average of the model m_1 over those cells, and $\bar{m}_2$ is the average of m_2. For computation, we take a suite of 5×3 cells to evaluate each correlation. Correlation values lie between $[-1, 1]$, so a DOI index in the range $[0, 1]$ can be defined by

$$R = \frac{C - 1}{2}. \quad (5)$$

The DOI index computed from models in Figures 5a and 5c is shown in Figure 6c. In Figure 6b, we plot this index directly on m^*; in Figure 6a, we use the DOI value to scale the color intensity of m^*. The DOI curves are quite compact in depth. This is due to the large gradients used for the background models.

Figures 4 and 6 provide two estimates of the DOI for this example. There are differences, but the depth at which R begins to change significantly is reasonably similar. Choosing the $R = 0.2$ contour on either plot would provide a sensible demarcation between features that are controlled by the data and

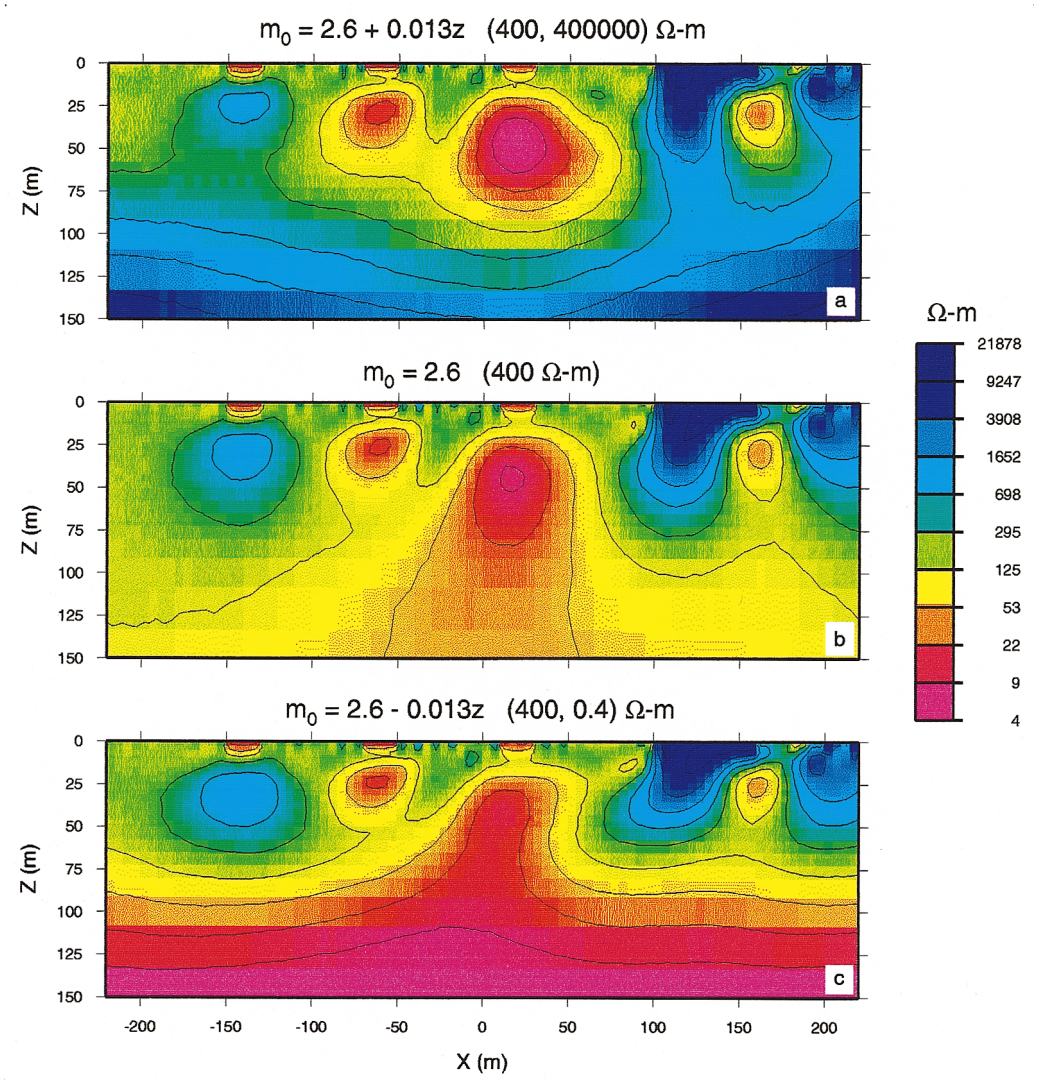

FIG. 5. Resistivity models generated using different ramp reference models. All inversions use coefficients $(\alpha_s, \alpha_x, \alpha_z) = (10^{-6}, 1, 1)$. The model in (b) is generated with a constant reference of 400 ohm-m, which has minimal effect due to the small α_s. This model is considered to be m^*. The resistivity in (a) is generated using a ramp reference model of the form $m_0 = c_0 + \gamma z$ where $\gamma = 0.013$. Thus the reference model is 400 ohm-m at the earth's surface and 400 000 ohm-m at the bottom of the mesh at 225 m. The resistivity in (c) is generated with a ramp reference model of the form $m_0 = c_0 - \gamma z$. The reference model is 400 ohm-m at the top and 0.4 ohm-m at the bottom of the mesh.

features that are controlled by the model objective function. Equivalently, Figures 4a and 6a provide the same essential information about the earth model.

In developing the background models needed to construct the DOI maps, we have found a number of models that fit the data to the same degree. All are generated so that they are smooth in the horizontal and vertical directions, but they are designed to be different in a large-scale sense. These models constitute a limited exploration of model space, and interpretations can be facilitated by viewing Figures 3 and 5 together. The similarities and differences are striking. All buried conductors and resistors are observed at approximately the same locations. Figure 5c shows that the large prism need not be closed. However, closure of the contours on the remaining bodies indicate they are confined bodies. Comparison of the six models immediately provides a great amount of information about depth of investigation. Also, by looking at differences between models one can obtain a visual estimate of a corridor where the data quickly lose ability to control the model. That is essentially what we are trying to estimate quantitatively with the DOI maps.

AN ALGORITHM FOR CONSTRUCTING DOI MAPS

We suppose that the user has designed an objective function of the form in equation (1) and specified constants $\alpha_s, \alpha_x, \alpha_z$ and an initial reference model m_0^* that we shall assume is a constant c_0. The next task is to determine the DOI map. This requires knowledge of the relative importance of α_s compared to α_x, α_z in the objective function. In the previous section, we outlined how to compute the DOI for two end-member cases: where α_s plays an important role in the objective function and where it does not. For many practical cases, the α_s for the primary inversion may be intermediate between these extremes. To evaluate this effect, we have carried out the inversions for our test model at different values of α_s and for two constant reference models $m_0 = 400$ ohm-m and $m_0 = 40$ ohm-m. We examine the recovered values of the model at three cell locations. The first cell has coordinates $(x, z) = (-127, 200)$ m. It lies towards the bottom of the mesh, and we expect that R is unity there. This is confirmed in Figure 7, where the model values from the inversions and the corresponding values of R

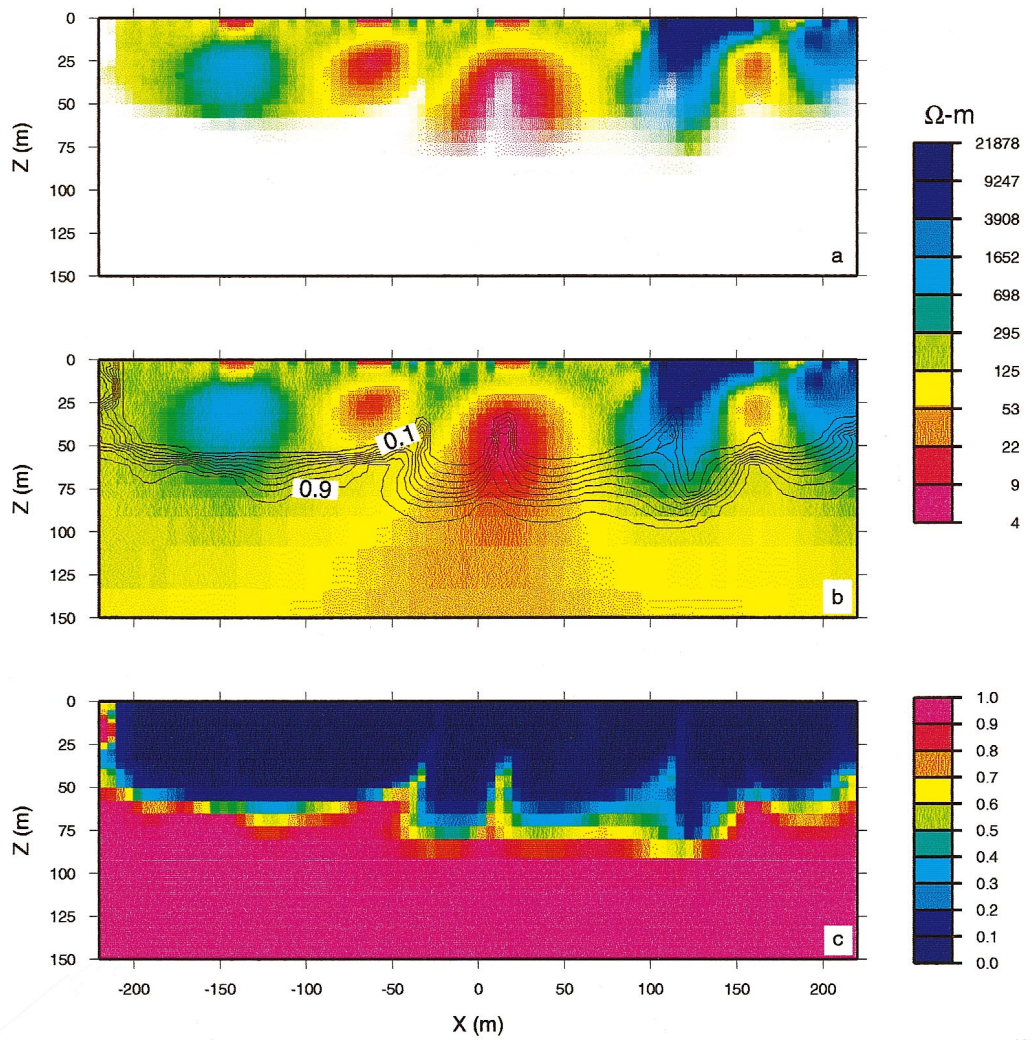

FIG. 6. The DOI index computed from inversions using ramp reference models is plotted in (c). These values are superposed on m^* in (b). The contour interval is 0.1. In (a) the intensity of m^* is scaled by the DOI value.

evaluated with equation (3) are provided. When α_s exceeds 10^{-2}, the recovered conductivity is approximately equal to the reference half-space and thus R is unity. However, as α_s decreases, the influence of the first component of the objective function lessens, and the recovered model becomes less dependent upon the reference. When α_s is less than 10^{-5}, the resistivities from both inversions are the same and are independent of the chosen value of the half-space.

The cell at $(x, z) = (-102, 100)$ m has similar characteristics although, even for large values of α_s, the recovered model does not quite achieve the reference half-space value. This is an indication that the conductivity in the cell is affecting the data and that R is less than unity. An entirely different behavior is observed for the cell at 37 m depth. This cell is well within the depth of investigation of the survey. Attempts to make the value of this cell equal to the background fail, even when α_s is large.

The curves in Figures 7a and 7c provide considerable insight. The importance of α_s in the inversion can be assessed by evaluating R at cells in which R should be unity. These are cells toward the bottom of the mesh. If R for those cells lie in the range $0.2 < R < 1.0$, then the inverted results are moderately dependent on α_s. We proceed by evaluating R using equation (3), but scale the results so that R at depth is unity. The validity of this is shown in Figure 8. The unscaled DOI curves are plotted on the left (Figures 8a–8c). Note that the first DOI contour ($R = 0.1$) progressively deepens as α_s becomes smaller. Scaling the DOI contours so that R is unity at the bottom of the mesh yields the results in Figures 8d–8f. The scale factors for $\alpha_s = 10^{-3}, 10^{-4}$, and 10^{-5} are, respectively, 1.12, 1.90, and 18.4. The results for $\alpha_s = 10^{-5}$ are surprisingly good despite the fact that the unscaled R was 0.05 towards the bottom of the model.

In practical applications, we proceed as follows. The halfspace reference model is perturbed and the inversion carried out. Equation (3) is used to evaluate R. If, for cells at the bottom of the mesh, $R_b > 0.2$, then α_s is assessed to be playing an significant role in the objective function, and a scaled value of R is used as the final DOI. If $R_b < 0.2$, then α_s is assessed to be playing an insignificant role in the objective function and thus character of the final model is determined primarily by the derivative terms. In this case, method 2 should be used to evaluate the DOI index. This requires two additional inversions.

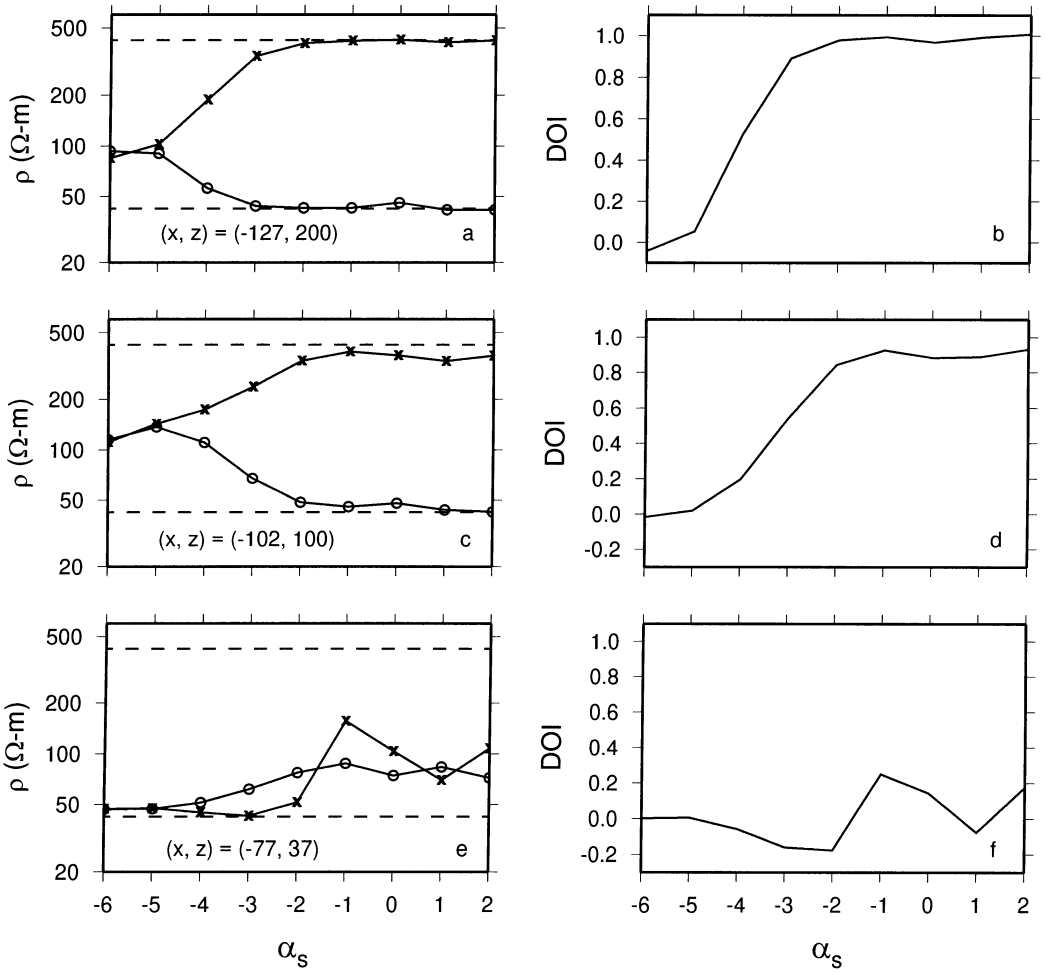

FIG. 7. The values of recovered resistivities at location $(x, z) = (-127, 200)$ as a function of α_s are shown in (a). The $\times$s are values obtained using a reference halfspace $m_{1r} = 400$ ohm-m and the os are obtained using the halfspace value $m_{2r} = 40$ ohm-m. The index R, evaluated using equation (3), is shown in (b). Only when α_s exceeds 10^{-2} does R approach unity. The results for a cell at $(x, z) = (-102, 100)$ are given in (c) and (d). That cell has minor influence on the data. The results for the cell at $(x, z) = (-77, 37)$ are substantially different. This corresponds to a depth which is well above the depth of investigation for the survey.

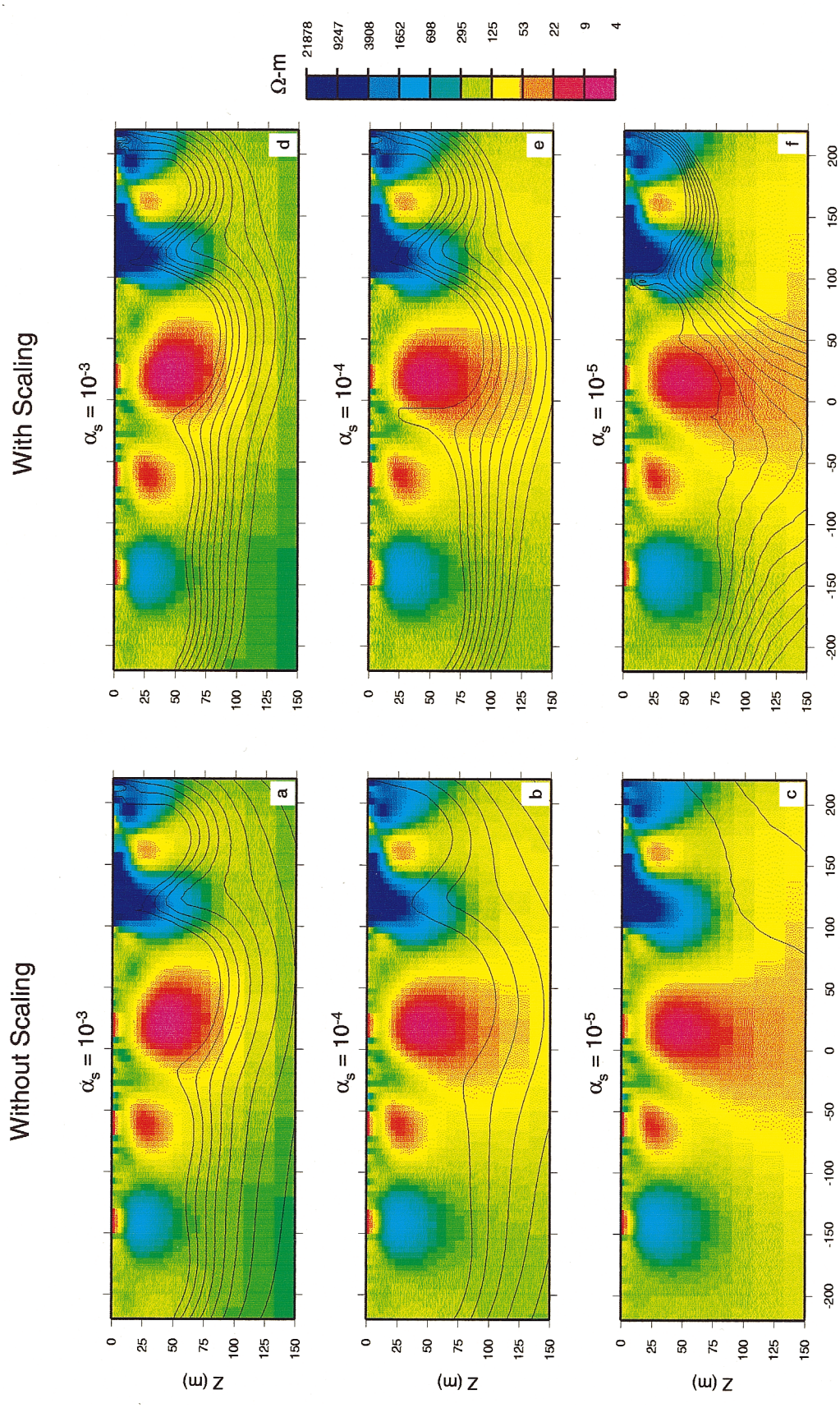

FIG. 8. The preferred models m^* generated using $\alpha_s = 10^{-3}$, 10^{-4}, and 10^{-5} are presented respectively in the top, middle, and bottom panels. Corresponding DOI curves, evaluated using equation (3), are plotted on the left. Note that the depth of the first contour ($R = 0.1$), deepens with decreasing α_s. After scaling according to equation (7), the inferred depth of investigation (on the right) is quite similar.

The explicit algorithm is

1) Choose $m_0 = \beta * c_0$.
2) Invert data to obtain m_1.
3) For cells at the bottom of the mesh, if

$$R_b = \frac{|m_1 - m^*|}{c_0(1-\beta)} > 0.2 \tag{6}$$

then: compute DOI index

$$R = \frac{|m_1 - m^*|}{R_b c_0(1-\beta)} \tag{7}$$

else

Ensure that the effect of α_s is minimal. Replace α_s by $\alpha_s * min(1, 10^{-3}/R_b)$.

Carry out two inversions with references models $m_0 = c_0 \pm \gamma z$. Evaluate R from equation (5).

end.

To employ the above algorithm, we need to determine parameters of the reference model. Method 1 evaluates the DOI by computing the difference between inversion results using two reference models $m_0^* = c_0$ and $\beta * c_0$. As with any finite differencing, if β is too close to unity, then results will not be reliable because of machine round-off errors. Questions also arise concerning whether the perturbed model should be more conductive or more resistive than m_0^*, and also whether one-sided or two-sided differences are preferable. We have attempted to address these questions empirically. Keeping $\alpha_s = 0.001$, inversions were carried out with $0.01 < \beta < 100$. One-sided differences from m_0^* and two-sided differences were computed. Overall, the final DOI maps were similar. The corridor along which the DOI index began to increase rapidly was noted to shift vertically by up to a few tens of meters for extreme models. However, these variations would not have altered the interpretation about assessing whether the individual structures were open or closed at depth. The DOI curves also are affected by the feature being analyzed. For instance, when analyzing a conductive target, shallower DOI curves are obtained if the perturbed model is made more resistive. Conversely for a resistive target, the DOI curves are closer to the surface if the reference model is made more conductive. Even fairly small changes in the reference model ($0.95 < \beta < 1.05$) produced good DOI maps. Extreme values of β, ($\beta = 0.01$ and $\beta = 100$) also produced reasonable estimates. Because of these results, and our desire to construct a model that is substantially different from m^*, we generally evaluate the DOI index using a reference model that differs from m_0^* by a factor of 5 to 10. If the feature of interest is a conductor, we make the new reference model more resistive, and if it is resistive, we make the new reference model more conductive.

Computing DOI maps using method 2 requires generating models with gradients that are $\pm\gamma$. If γ is small, the DOI curves are spread out in depth. They get closer together as γ increases. Despite the differences in details, the DOI maps obtained from different γs provided consistent information in this example to assess whether the buried conductors and resistors were open or closed at the depth of investigation limit. To construct DOI maps, and also to have additional models to interpret, we have generally selected γ such that the reference conductivity changes by a factor of 5 to 10 over a depth range equal to L, where L is the length of the array.

We want to emphasize that our procedure provides information only about the corridor in which the data become insensitive to the earth model. Small details in any particular DOI contour should not be interpreted and, for presentation purposes, some additional smoothing might be desirable if contour lines are presented. We have not done that here.

DEPTH OF INVESTIGATION FOR DIFFERENT ARRAY CONFIGURATIONS

Considerable research has been devoted to examining the relative merits of using different electrode arrays in geophysical surveys. General rules of thumb advocate that dipole-dipole data have the greatest near-surface resolving power but see the shallowest. Pole-pole data have the poorest resolution but see the deepest. Pole-dipole data are intermediate. In principle, pole-pole data, which are the most primitive data set, contain the most information about the earth model. Data from any other electrode configuration can be generated by taking linear combinations of the pole-pole data, although for field data there are adverse implications regarding signal-to-noise (Beard and Tripp, 1995). The reverse is not true, however; pole-pole data cannot be obtained from dipole-dipole data. Inherently then, dipole-dipole data must have less information about the earth than do pole-pole data. An additional, and critical, aspect in comparison of resolving power or depth of investigation of different arrays, is data error. Resolving power and depth of investigation of any experiment depends upon the accuracy of the data. The larger the errors, the more poorly we resolve features at depth. This aspect cannot be overemphasized.

If the noise is specified, then the depth of investigation of different arrays can be compared by evaluating the DOI maps. This is not the main thrust of our paper, but we present one analysis to illustrate how the comparisons can be carried out. Simulated data from pole-pole, pole-dipole, and dipole-dipole surveys over our model are provided in Figure 9. Uncorrelated Gaussian random noise with a standard deviation equal to 5% of the datum magnitude and a base level have been added to the data. The base level is proportional to the signal strength of each data set such that all four data sets have approximately the same signal-to-noise ratio. The pseudosections are dominated by linear features that are directly related to electrode geometry. The pole-pole data appear to be less influenced by the near-surface conductors and may see the large deep conductor in the middle. The image is smooth compared to that from the dipole-dipole pseudosection. These visual differences, however, are mainly caused by the geometry of data collection, and they do not directly convey the relative information about the conductivity structure that is encoded in the data. That can be done only through inversion.

Figures 9e–9h show the recovered models obtained by inverting the resistivity pseudosections with $(\alpha_s, \alpha_x, \alpha_z) = (0.001, 1, 1)$ and a half space reference model of 400 ohm-m. Most noticeable is that the recovered models provide similar information about the earth resistivity structure. The distortions in the pseudosection caused by electrode geometry are absent in the inverted models. This is in accordance with an understanding that the different data sets can all be made up of the fundamental pole-pole data set and that they therefore have

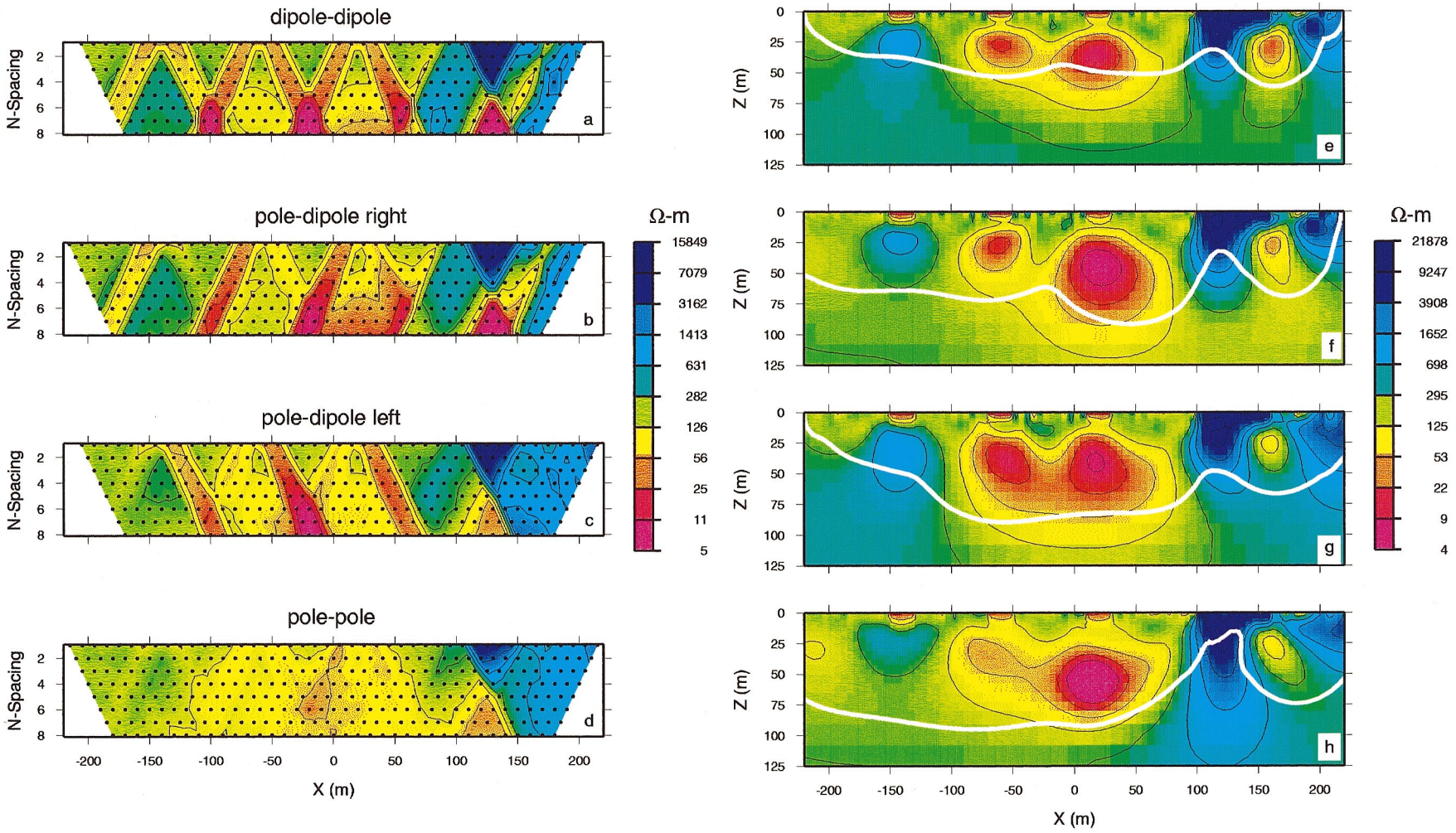

FIG. 9. Pseudo sections of dipole-dipole, pole-dipole right (potential electrodes to the right of the current), pole-dipole left (potential electrodes to the left of the current), and pole-pole are plotted respectively in (a)–(d). The data have been contaminated with noise. The resistivity models recovered from the inversion are displayed on the right, and a DOI index curve corresponding to $R = 0.2$ has been plotted on each figure. With the errors provided, dipole-dipole data have a smaller depth of investigation than the other arrays. Note, however, that different electrode arrays give rise to approximately the same information about conductivity even though their pseudosection representations are substantially different.

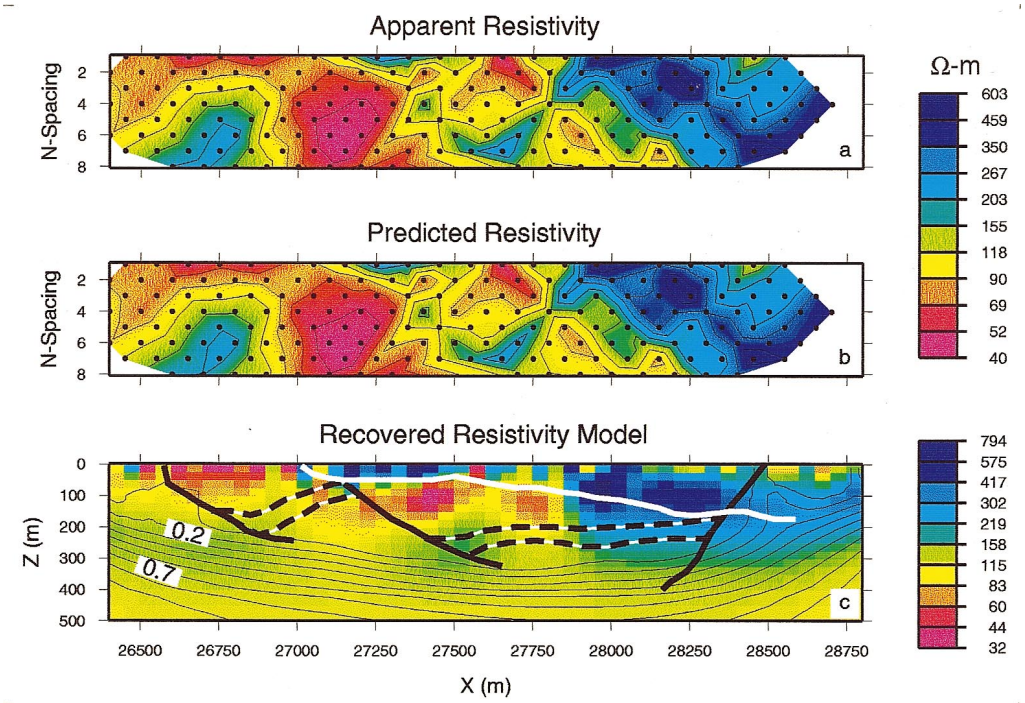

FIG. 10. Apparent resistivity data from the Century deposit are shown in (a). The predicted data are in (b). The model recovered from the inversion is in (c) with DOI curves superposed. The top contour is $R = 0.1$. The white line is the depth of the overburden obtained from drill logs. The logs also provided estimates for the top and bottom of the ore zone (dashed lines) and the faults (solid black lines).

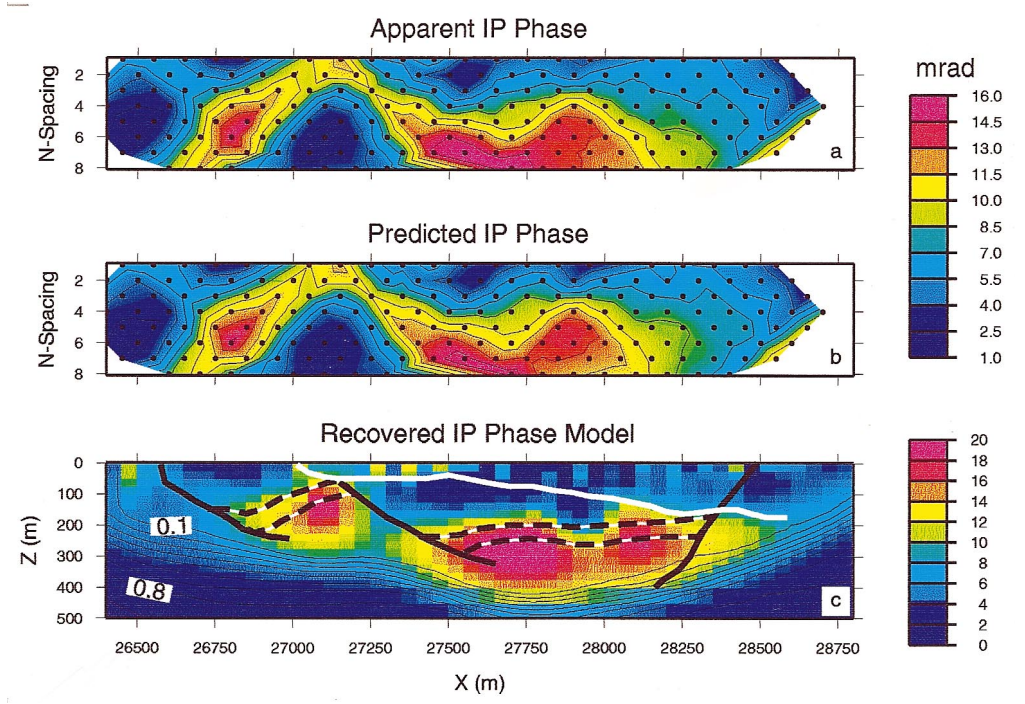

FIG. 11. Apparent phase data from the Century deposit are shown in (a). The predicted data are in (b). The model recovered from the inversion is in (c) with the DOI curves superposed. The top contour value is $R = 0.1$. The white, dashed, and solid lines are the same as those in Figure 10.

the same information about the earth embedded in them. On a more detailed level, the near-surface conductivity is equally well delineated, but the depth extent of features in the dipole-dipole data is less than for that from the pole-pole data set. The pole-pole results indicate a loss of lateral resolution in that the separation of the large and small conductor is blurred. Also buried bodies are slightly deeper. These differences between the recovered models result primarily because of the choice of noise levels for the data and because no data set can be exactly reproduced by a linear combination of data from another array.

The white line on each figure is the DOI index curve corresponding to the $R = 0.2$ contour value. To evaluate that line, we re-inverted the data with a reference of 40 ohm-m. The contour values were scaled so that $R = 1$ at the bottom. The DOI contours have similar shape but there is a difference in depth. The contour is shallowest for the dipole-dipole data, and it is no longer clear that the resistive prism on the left is closed. The contour for the pole-dipole, with the potential dipole on the left, also intersects the resistor. This loss of depth information in that area is due to recording geometry, as can be seen by comparing with the results from pole-dipole right.

FIELD EXAMPLE

As a field example, we apply our strategy to a data set from the Century deposit in Australia. Complex resistivity dipole-dipole data with $a = 100$ m and $n = 1 \ldots 8$ were collected. The dc resistivity data, recovered model, and predicted data are provided in Figure 10. The inverted model was obtained by assuming 5% noise on the data and setting $(\alpha_s, \alpha_x, \alpha_z) = (0.001, 1, 1)$. The reference model is a half-space of 100 ohm-m. The primary benefit of the dc resistivity interpretation has been to delineate the thickness of the resistive overburden. The DOI curves were computed after carrying out another inversion with a reference of 1000 ohm-m. The DOI curve for $R = 0.2$ approaches 100 m or less at the two ends of the survey and extends to about 300 m in the middle. This is greater than the depth of the orebody delineated by the dashed line.

The DOI analysis can be applied to IP data. For the primary inversion, we assume the reference model is zero. The chargeability data, recovered model, and predicted data are shown in Figure 11. The IP inversion has delineated the horizontal extent of, and depth to, the orebody. It also indicates a major fault between $x = 27\,000$ m and $x = 27\,500$ m, which dislocates the ore sequence. To calculate the DOI curves, we perform another inversion with a reference model of 10 mrad. The $R = 0.2$ contour lies significantly below the portion of the orebody at the left and closure of that feature is inferred. This is consistent with drill information. The interpretation is less clear for the central deeper orebody, but the DOI curves all lie significantly below the maximum, and this suggests that the body is confined in depth.

CONCLUSIONS

Once data have been properly prepared, the major manual effort needed to invert geophysical data centers around the decision of what objective function is to be minimized and how well to fit the data. The inversion algorithm then provides a model from which final interpretations can be made. To assess whether features at depth are demanded by the data or are artifacts of the inversion process, we need to quantify the depth of investigation that is inherent to any survey. Our approach is to alter the model objective function, carry out a subsequent inversion, and then observe the differences between models. Locations where large differences occur are clearly areas where the data do not constrain the model. A DOI index that has the range [0, 1] quantifies the change. Latitude exists regarding how the objective function can be altered. We have chosen only to alter the reference model m_0. If the objective function that produced m^* was dominated by the "smallest" model term (controlled by α_s), we suggest altering the reference model by a significant factor (say a factor of 5–10). If the objective function is controlled by terms that minimize horizontal and vertical variation, then we suggest two additional inversions in which the reference model has strong positive and negative gradients. In practise, we advocate that all three of these inversions be carried out prior to final interpretation. This requires extra CPU time, but the procedure is not manually intensive. Plots of three or four models which, at depth, are significantly different from our "best" result are extremely informative in the interpretation. Visual examination of these plots can provide an estimate of a depth corridor below which model features are no longer controlled by the data. The DOI maps quantify this depth and ultimately prevent overinterpretation of inversion results.

ACKNOWLEDGMENTS

We thank Roman Shekhtman for carrying out the inversion runs required to generate the results in this paper. We also thank Theo Aravanis of CRAE for providing the Century data. Reviews by David Alumbaugh, Les Beard, Craig Beasly, and an anonymous referee greatly improved our paper. This work was supported by an NSERC IOR grant and an industry consortium "Joint and Cooperative Inversion of Geophysical and Geological Data." Participating companies are Placer Dome, BHP Minerals, Noranda Exploration, Cominco Exploration, Falconbridge, INCO Exploration & Technical Services, Hudson Bay Exploration and Development, Kennecott Exploration Company, Newmont Gold Company, Western Mining Corporation, and CRA Exploration Pty.

REFERENCES

Apparao, A., Rao, T. G., Sastry, R. S., and Sarma, V. S., 1992, Depth of detection of buried conductive targets with different electrode arrays in resistivity prospecting: Geophys. Prosp. **40**, 749–760.
Barker, R. D., 1989, Depth of investigation of colinear symmetrical four-electrode arrays: Geophysics, **54**, 1031–1037.
Beard, L. P., and Tripp, A. C., 1995, Investigating the resolution of IP arrays using inverse theory: Geophysics, **60**, 1326–1341.
Edwards, L. S., 1977, A modified pseudosection for resistivity and IP: Geophysics, **42**, 1020–1036.
Evjen, H. M., 1938, Depth factors and resolving power of electrical measurements: Geophysics, **3**, 78–95.
Oldenburg, D. W., 1978, The interpretation of direct current resistivity measurements: Geophysics, **43**, 610–625.
Oldenburg, D. W., and Li, Y., 1994, Inversion of induced polarization data: Geophysics, **59**, 1327–1341.
Parker, R. L., 1984, The inverse problem of resistivity sounding: Geophysics, **49**, 2143–2158.
Roy, A., 1972, Depth of investigation in Wenner three-electrode and dipole-dipole dc resistivity methods: Geophys. Prosp., **20**, 329–340.
Roy, A. and Apparao, A., 1971, Depth of investigation in direct current methods: Geophysics, **36**, 943–959.
Van Nostrand, R. G., 1953, Limitations on resistivity methods as inferred from the buried sphere problem: Geophysics, **18**, 423–433.